RSC Advances

ROYAL SOCIETY OF CHEMISTRY

www.rsc.org/advances

Table of Contents

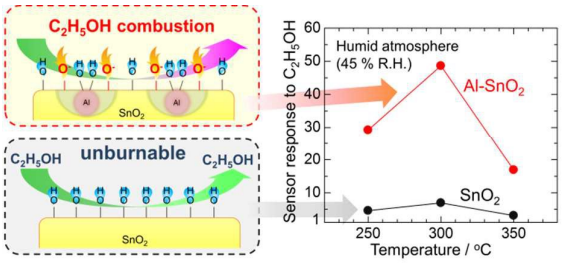

Aluminium-doped SnO_2 nanoparticles inhibited a hydroxyl poisoning and enhanced the sensor response in humid atmosphere

Journal Name

ARTICLE

Surface-modification of SnO_2 nanoparticles by incorporation of Al for the detection of combustible gases in humid atmosphere

Received 00th January 20xx,
Accepted 00th January 20xx

DOI: 10.1039/x0xx00000x

www.rsc.org/

Koichi Suematsu†[a], Nan Ma[b], Masayoshi Yuasa‡[a] , Tetsuya Kida[c], Kengo Shimanoe[a]

Inhibition of hydroxyl poisoning of SnO_2 nanoparticles is important to develop a highly sensitive combustible gas sensor that functions in a humid atmosphere. For this purpose, we incorporated Al into SnO_2 nanoparticles (Al-doped SnO_2) by a precipitation method, and fabricated a thick-film-type sensor using a screen printing method. Bare SnO_2 nanoparticles and Al_2O_3-loaded SnO_2 nanoparticles were also prepared for comparison. The oxygen adsorption amount clearly decreased after Al doping and Al_2O_3 loading, according to temperature programmed desorption measurements. Al doping enhanced the sensor response (sensitivity) to H_2, CO and C_2H_5OH in a humid atmosphere by almost five to ten times. Al_2O_3 loading also slightly increased the sensor response to each gas in a humid atmosphere. The enhancement of the sensor response was attributed to both Al and Al_2O_3 acting as hydroxyl absorbers on the surface of the nanoparticles, thereby providing an oxygen adsorption site for surface combustion reactions in a humid atmosphere. Based on the relationship between the sensor response and C_2H_5OH concentration, it was estimated that Al-doped SnO_2 can detect less than one ppm C_2H_5OH in a humid atmosphere. Therefore, doping with Al, which protects and holds the adsorbed oxygen on the surface of the SnO_2, is important as a surface modification to obtain humidity-tolerant semiconductor gas sensors.

Introduction

Tin dioxide (SnO_2) is well known as one of the multifunctional material having a wide applications such as gas sensors [1-6], catalyst [6-8], optoelectronic device [4,5,9-11], and so on [4,5,12]. In particular, SnO_2 based semiconductors offer great potential for gas sensors because of their detection accuracy and high sensitivity to combustible gases. For example, we developed a highly sensitive H_2S gas sensor using crystallite controlled SnO_2 nanoparticles [1] and a highly sensitive volatile organic compounds (VOCs) gas sensor using clustered (aggregated) Pd/SnO_2 nanoparticles [2]. Such SnO_2-based gas sensors allow instant gas detection because SnO_2 responds rapidly to combustible gases [13]. Moreover, compact and low-power gas sensors have recently been investigated for battery-operated portable devices [14,15]. However, the potential of these gas sensors has often been demonstrated in a dry atmosphere because SnO_2 has a significantly low tolerance to humidity. Therefore, many researchers are interested in humidity-tolerant materials as semiconductor gas sensors for monitoring the gas components.

SnO_2-based semiconductors have been recognized as a promising material because of their sensitive response to combustible gases. However, SnO_2 is vulnerable to humidity because of its gas detection mechanism. Normally, the electric resistance of SnO_2 is strongly dependent on the presence of negatively charged adsorbed oxygen on the particle surface, as explained below.

$$O_2 + 2e^- \rightarrow 2O^-_{ad} \quad (1)$$

Here e^- is a carrier electron in SnO_2 and O^-_{ad} is adsorbed oxygen trapping the electron. This reaction leads to the formation of an electron depletion layer on the particle surface and an increase in the electric resistance. Combustible gases, such as H_2, are detected by a combustion reaction with adsorbed oxygen on the SnO_2 surface. This reaction is shown in the following equation.

$$H_2 + O^-_{ad} \rightarrow H_2O + e^- \quad (2)$$

Consequently, the electric resistance decreases as the electron depletion layer is reduced by the release of the trapped electrons. The difference in the electric resistance is used as a signal for gas detection. However, oxygen adsorption on the SnO_2 surface is strongly disturbed by hydroxyl poisoning in a humid atmosphere [16-19]. Therefore, detection of combustible gases in a humid atmosphere is difficult. In a commercial gas sensor, the sensing layer is capped by a humidity absorber, such as activated carbon, to avoid hydroxyl poisoning. To develop reduced-size semiconductor gas sensors, it is desirable that the semiconductor materials are resistant to humidity.

[a] *Department of Energy and Material Sciences, Faculty of Engineering Science, Kyushu University, Kasuga, Fukuoka, 816-8580, Japan.*
E-mail: k.suematsu.5638@gmail.com, Fax: +81-92-925-7724
[b] *Department of Molecular and Material Science, Interdisciplinary Graduate School of Engineering Science, Kyushu University, Kasuga, Fukuoka, 816-8580, Japan.*
[c] *Department of Applied Chemistry and Biochemistry, Kumamoto University, Kumamoto, 860-8555, Japan.*
†Current address: *Present address: Chemical and Texture Research Institute, Fukuoka Industrial Technology Center, Chikushino, Fukuoka, 818-8540, Japan.*
‡Current address: *Department of Biological and Environmental Chemistry, School of Humanity-Oriented Science and Engineering, Kinki University, Iizuka, Fukuoka 820-8555, Japan*

Recent research has focused on protecting the sensor from deterioration due to hydroxyl poisoning. For example, it has been accepted that catalytic Pd loading on the SnO_2 particle leads to less hydroxyl poisoning [18,19]. We found that the main oxygen adsorption species of SnO_2 and Pd-loaded SnO_2 were O^- and O^{2-} in a humid atmosphere [20]. Accordingly, O^{2-} on PdO prevented hydroxyl adsorption on the SnO_2 surface. Furthermore, Kim et al. proposed that NiO, a humidity absorber, protects the SnO_2 surface from hydroxyl poisoning according to the results of their diffusion-reflectance Fourier transform IR (DRIFT) spectroscopy measurements [21]. Moreover, Choi et al. reported that CuO also worked as a humidity absorber on the SnO_2 surface for H_2S sensing in a humid atmosphere. They proposed that CuO is effective because it has a high affinity towards water vapour [22]. Therefore, protecting and holding adsorbed oxygen on the SnO_2 surface is the key to producing a high performance gas sensor in a humid atmosphere.

In this study, we attempted to enhance the sensor response to combustible gases in a humid atmosphere by using SnO_2-based semiconductor gas sensors. Aluminium ions and alumina, which have a high affinity for water and hydroxyl adsorption [23-25], were incorporated into SnO_2 nanoparticles to protect the adsorbed oxygen. To investigate the effect of surface modification on the oxygen and hydroxyl adsorption, we prepared conventional spherical bare-SnO_2 nanoparticles, Al-doped SnO_2 nanoparticles, and Al_2O_3-loaded SnO_2 nanoparticles. Sensor responses to combustible gases H_2, CO, and C_2H_5OH in dry and humid atmospheres were investigated by analysing the electric resistance with considering their crystallite size, specific surface area, pore radius, and amount of oxygen adsorbed. It is noteworthy that Al-doped SnO_2 showed a high response to C_2H_5OH in a humid atmosphere even though its crystallite size, specific surface area, and pore radius were almost the same as bare-SnO_2. These results show that the developed semiconductor gas sensors can be used in a humid atmosphere without capping and could lead to the development of more compact sensor devices.

Experimental

Material preparation

Bare-SnO_2 nanoparticles were prepared using a hydrothermal treatment, as reported previously [2]. Stannic acid gel was prepared by adding an aqueous solution of $SnCl_4 \cdot 5H_2O$ (1M) dropwise into a NH_4HCO_3 solution (1M). The aqueous dispersion of the stannic acid gel was hydrothermally treated at 200 °C for 3 h at 10 MPa with continuous stirring at 600 rpm, after removal of Cl^- by centrifugation. To prepare a monodispersed solution of smaller SnO_2 nanoparticles, the pH of the solution was adjusted to 10.6. The solution was dried at 120 °C for 6 h and calcined at 600 °C for 3 h to produce a powder of bare-SnO_2 nanoparticles.

Al (0.5 mol%)-doped SnO_2 nanoparticles were prepared by a conventional precipitation method, reported previously [26]. $SnCl_4 \cdot 5H_2O$ and $AlCl_3$ were used as the starting materials. An appropriate amount of a mixed aqueous solution of $SnCl_4$ and $AlCl_3$ was added dropwise into a NH_4HCO_3 solution. After waiting for 12 h to obtain a white precipitate, the hydroxide gel was washed and the Cl^- was removed by centrifugation. The gel was dried at 120 °C and calcined at 600 °C for 3 h to obtain a powder of Al-doped SnO_2 nanoparticles.

For comparison with Al-doped SnO_2, we prepared Al_2O_3 (0.5 mol% Al atom)-loaded SnO_2 nanoparticles using an impregnation method [26]. Carrier SnO_2 nanoparticles were prepared using a conventional precipitation method, in the same manner as the Al-doped SnO_2. The stannic acid gel was prepared by adding a $SnCl_4$ aqueous solution (1M) into NH_4HCO_3 solution (1M). The precipitated white gel was dried at 120 and calcined 600 °C for 3 h to obtain the carrier SnO_2 powder, after removing Cl^- from the gel by centrifugation. The obtained powder was dispersed in deionized water and $Al(NO_3)_3$ (0.5 mol%) was added to the solution by stirring. The Al_2O_3-loaded SnO_2 nanoparticles powder was obtained by evaporating the solution at 100 °C and calcining the dried powder at 600 °C for 3 h.

Preparation of the sensor device and evaluation of the electric resistance

A screen printing method was used to mount the SnO_2-based powders on an alumina substrate (9 × 13 × 0.38 mm), which was printed with an Au comb-type electrode (180-μm line width, 90-μm distance between lines, 64-mm^2 sensing area). For screen printing, an SnO_2 paste was prepared by mixing the SnO_2-based powders with α-terpineol. The sensing films were deposited on the substrates and sintered at 580 °C for 3 h with flowing synthetic air. The air was controlled using a conventional gas-flow apparatus equipped with an electric furnace (Fig. 1). The flow rate of the synthetic air and sample gases was kept at 80 cm^3/min by mass flow controllers (SEC-series; HORIBA STEC). Sample gases of H_2, CO, and C_2H_5OH in air were prepared by diluting the parent synthetic gas mixtures with synthetic air. A humid atmosphere was prepared by blowing the sample gases into pure water (Fig. 1), and humidity was determined using a commercial humidity sensor (TR-77Ui; T&D Corporation). Each sensor device was connected with a standard resistor in series. Voltage across the standard resistor was measured under an applied DC voltage of 4 V to evaluate the electric resistance of the sensors. An electric signal was acquired using an electrometer (2701; Keithley Instruments). The sensor response (S) was defined as the ratio of the electric resistance in air (R_a) to the resistance in the sample gases (R_g) ($S = R_a/R_g$).

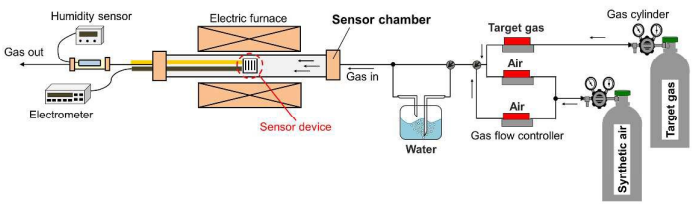

Fig. 1 Schematic image of a gas flow apparatus with an electrical measurement system.

Results and discussion

Material characterization

XRD patterns of the bare-SnO_2, Al-doped SnO_2 (Al-SnO_2), and Al_2O_3-loaded SnO_2 (Al_2O_3-SnO_2) nanoparticles are shown in Fig. 2a. The obtained XRD patterns correspond well with the cassiterite structure of SnO_2 (JCPDS: 41-1445) and no impurity peaks were observed. The estimated crystallite size of each nanoparticle is shown in Table 1. The crystallite size of bare-SnO_2 and Al-SnO_2 were similar sizes, 14 and 12 nm, respectively. The average crystallite size of bare-SnO_2 prepared using the same conventional precipitation process as for Al-SnO_2, was almost 18 nm. Al doping reduces the crystallite size of SnO_2 nanoparticles. It is well accepted that metallic ion doping inhibits the crystal growth of SnO_2 [9,26]. This is the slight evidence that Al is doped into the SnO_2 nanoparticles. A small peak shift of the XRD patterns would also indicate doping of other elements, as reported by Duan et al. [9]. However, no peak shifts in the XRD patterns were observed because the amount of Al doping was very low. In the case of Al_2O_3-SnO_2 nanoparticles, the crystallite size of 19 nm was larger than the other materials because the size of the carrier SnO_2 was 18 nm. TEM images of the nanoparticles are shown in Fig. 2b-d, and spherical type SnO_2 crystals were observed in each image. The Al_2O_3-SnO_2 nanoparticles were discernibly larger than the other nanoparticles. The observed crystallite size of bare-SnO_2, Al-SnO_2, and Al_2O_3-SnO_2 were 14, 13, and 22 nm, respectively. These were similar to the crystallite sizes estimated from the XRD patterns.

Table 1 Estimated values of average crystallite size (XRD), specific surface area (BET), peak pore radius (BJH) and O_2 desorption amount (O_2-TPD) for bare-SnO_2 nanoparticles, Al-doped SnO_2 nanoparticles, and Al_2O_3-loaded SnO_2 nanoparticles.

Sample	Ave. crystallite size / nm	Specific surface area / $m^2 \cdot g^{-1}$	Peak pore radius / nm	O_2 desorption	
				/ $\mu mol \cdot g^{-1}$	/ $\mu mol \cdot m^{-2}$
Bare-SnO_2	14	26.5	10.8	21	0.78
Al-SnO_2	12	26.2	9.3	10	0.39
Al_2O_3-SnO_2	19	15.7	14.3	8.0	0.51

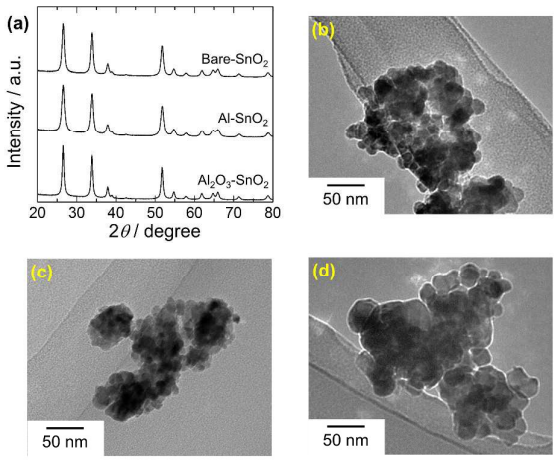

Fig. 2 (a) XRD patterns of nanoparticles and TEM images of (b) bare-SnO_2 nanoparticles, (c) Al-doped SnO_2 nanoparticles, and (d) Al_2O_3-loaded SnO_2 nanoparticles.

The pore size distribution of each nanoparticles is shown in Fig. 3a, and the estimated specific surface area and peak pore radius are shown in Table 1. Bare-SnO_2 and Al-SnO_2 nanoparticles had a comparable specific surface area and peak pore radius. Al_2O_3-SnO_2 had a smaller specific surface area and a larger peak pore radius because of a larger crystallite size and particle aggregation. SEM images of each nanoparticles on the sensing layer are shown in Fig. 3b-d. The observed pore and particle size of bare-SnO_2 was comparable in size to Al-SnO_2. However, Al_2O_3-SnO_2 had larger nanoparticles and pores than bare-SnO_2. Both the bare-SnO_2 and Al-SnO_2 nanoparticles accumulated in a dense packing layer with small particles, whereas the Al_2O_3-SnO_2 nanoparticles accumulated in a loose packing layer. Thereby, we can investigate the Al doping effect without considering particle size and morphology.

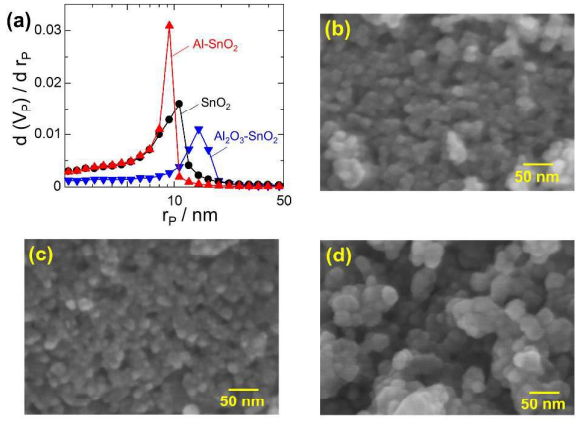

Fig. 3 (a) Pore radius distributions of each nanoparticles and SEM images of (b) bare-SnO_2 nanoparticles, (c) Al-doped SnO_2 nanoparticles, and (d) Al_2O_3-loaded SnO_2 nanoparticles.

Figure 4 shows the O_2-TPD results of bare-SnO_2, Al-SnO_2, and Al_2O_3-SnO_2 nanoparticles. Two large peaks were observed at 100 and 450 °C; these were attributed to desorption of adsorbed molecular oxygen (O_2^-) and adsorbed dissociated oxygen with a negative charge (O^- or O^{2-}), respectively [17]. The adsorbed oxygen (O^- or O^{2-}) peaked at 450 °C is attributed to the surface reaction (Equation 2) that causes decreasing of

adsorbed oxygen amount because of the H_2O emission evaluation [17,20]. We estimated the oxygen desorption amount in the range of 350-520 °C from the amount of adsorbed oxygen using Fig. 4, and listed these values in Table 1 as two different units, μmol·g^{-1} and μmol·m^{-2}. Bare-SnO_2 desorbed almost two times more adsorbed oxygen (O^- or O^{2-}) than Al-SnO_2 and Al_2O_3-SnO_2. In previous reports of TPD measurements, Huang et al. revealed that the oxygen desorption peak was observed at approximately 527 °C (800 K) when using γ-Al_2O_3 [27]. Moreover, Putna et al. reported that no oxygen desorption peak was observed using α-Al_2O_3 (0001) [28]. These results indicate that the presence of Al decreases the oxygen desorption amount because of the reduction of naked oxygen adsorption sites in SnO_2. The oxygen desorption amount per unit area, μmol· m^{-2}, of Al-SnO_2 was smaller than Al_2O_3-SnO_2. Usually, the naked surface area of the carrier material decreases with an increase in dispersity of the doping or loading element. Thus, the Al in Al-SnO_2 was more dispersed on the surface than the Al_2O_3 in Al_2O_3-SnO_2, and the Al in Al-SnO_2 effectively disturbed oxygen adsorption on the SnO_2 surface. Therefore, Al doping and Al_2O_3 loading decreased the oxygen adsorption on the SnO_2, and Al was probably highly dispersed in the SnO_2 nanoparticles.

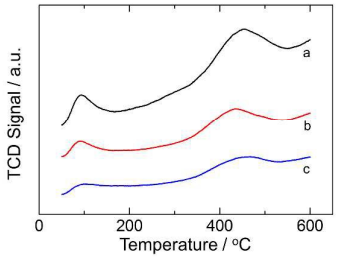

Fig. 4 Oxygen desorption spectra of O_2-TPD measurement using (a; black line) bare-SnO_2 nanoparticles, (b; red line) Al-doped SnO_2 nanoparticles, and (c; blue line) Al_2O_3-loaded SnO_2 nanoparticles.

The electric resistance in synthetic air

The electric resistance of SnO_2 nanoparticles is greatly influenced by the change in the oxygen adsorption amount [5] and other element doping [26,29] and loading [20,22,26]. Figure 5a and b show the electric resistance in synthetic air in dry and humid (45% R.H. at 25 °C) atmospheres, respectively. In a dry atmosphere, Al-SnO_2 and Al_2O_3-SnO_2 showed higher electric resistance than bare-SnO_2. In previous work, we prepared Fe-doped SnO_2 nanoparticles using the same process as with Al-SnO_2, and we confirmed that Fe doping into SnO_2 nanoparticles increases their electric resistance [26]. Hence, increasing the electric resistance of Al-SnO_2 was attributed to the replacement of Sn^{4+} with Al^{3+}, leading to a decrease in the donor density. Conversely, mixing Al_2O_3 with SnO_2 prevents electron transport between the SnO2 nanoparticles and increases the electric resistance. This occurs because Al_2O_3 is an insulating material. The amount of oxygen adsorbed by Al-SnO_2 and Al_2O_3-SnO_2 was less than the bare-SnO_2, as shown in Fig. 4. Therefore, Al doping and Al_2O_3 loading were effective at increasing electric resistance.

In a humid atmosphere, the electric resistance of each sensor decreased (Fig. 5b). It is well accepted that oxygen adsorption is disturbed by hydroxyls adsorbed on the oxygen adsorption site. Al-SnO_2 and Al_2O_3-SnO_2 nanoparticles showed a higher electric resistance than bare-SnO_2 nanoparticles, even in a humid atmosphere. The reason for the high electric resistance was caused less by oxygen adsorption and more by Al doping and Al_2O_3 loading. Sensor response to water vapour, which is the ratio of electric resistance in dry air to that in humid air, is shown in Fig. 5c. Sensor response increased with decreasing operating temperature in all samples because hydroxyl poisoning increases with decreasing temperatures. Bare-SnO_2 nanoparticles was clearly more sensitive to humidity than Al-SnO_2 and Al_2O_3-SnO_2 nanoparticles at 250 °C because there are fewer oxygen adsorption sites on Al-SnO_2 and Al_2O_3-SnO_2 than on bare-SnO_2. In addition, our SnO_2-based nanoparticles had a high affinity for hydroxyls.

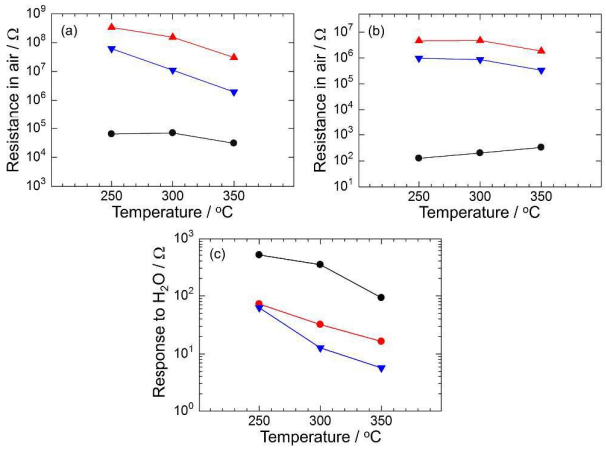

Fig. 5 Temperature dependence of the electric resistance in synthetic air atmosphere (a) in dry and (b) humid (45 % R.H. at 25 °C), and (c) the response to humidity using (●) bare-SnO_2 nanoparticles, (▲) Al-doped SnO_2 nanoparticles, and (▼) Al_2O_3-loaded SnO_2 nanoparticles.

The sensor response to combustible gases

The sensor response to combustible gases was examined using bare-SnO_2, Al-SnO_2, and Al_2O_3-SnO_2 nanoparticles. The sensor response relies on the surface reaction between adsorbed oxygen and combustible gases, so the amount of oxygen adsorbed strongly affect sensor response. Yamazoe et al. proposed a theoretical approach for estimating sensor response and suggested the following equation to represent the hydrogen response [30]:

$$S^2 = (R_a/R_g)^2 = (3c/aN_d)\cdot P_{H2} + \text{const.} \quad (3)$$

Here $c = k_2/k_{-1}$ is the constant, k_2 is the rate constant of forward reaction of equation (2), k_{-1} is the rate constant of the reverse reaction of equation (1), a is the crystal radius, N_d is the donor density of SnO_2, and P_{H2} is the partial pressure of hydrogen. According to this equation, reduction of donor density and crystallite size enhances sensor response to H_2. We have confirmed experimentally that the equation holds true for donor density reduction [26]. However, in the case of Al-SnO_2, there was a reduction in not only the donor density but also the oxygen adsorption amount. According to the equation, these two factors should have an opposite influence on the sensor response.

The temperature dependence of the sensor response to 200 ppm of H_2, 200 ppm of CO, and 100 ppm of C_2H_5OH in a dry atmosphere is shown in Fig. 6a, b, and c, respectively. In response to H_2 and CO, the sensor response using bare-SnO_2

nanoparticles went through a maximum at 300 °C. Such volcano-shaped behaviour is typical of a SnO_2 sensor and can be explained theoretically by the surface reactions and gas diffusion of SnO_2 [31]. Al-SnO_2 and Al_2O_3-SnO_2 showed a high sensor response at 250 °C even though Al and Al_2O_3 are not strong catalytic materials for surface reactions. The surface combustion reaction makes byproducts H_2O and CO_2, and these byproducts are adsorbed on the oxygen adsorption site and inhibit oxygen re-adsorption. Accordingly, the sensor response is further increased. At an optimum temperature, the surface reaction activity, gas diffusion, and adsorption/desorption of byproducts are balanced to give the highest possible sensor response. The adsorption capability of the byproducts was probably higher for Al-SnO_2 and Al_2O_3-SnO_2 than bare-SnO_2 at lower temperatures. The maximum sensor response to H_2 and CO of bare-SnO_2 was higher than to Al-SnO_2 and Al_2O_3-SnO_2. As mentioned above, the sensor response is related not only to the oxygen adsorption amount but also to the crystallite size and donor density. In both the sensor responses of bare-SnO_2 and Al-SnO_2, the oxygen adsorption amount had more effect on the sensor response than the donor density. Thus, the reduced sensor response to Al-SnO_2 and Al_2O_3-SnO_2 was mainly attributed to the reduction of oxygen adsorption sites on the particle surface. The sensor response to C_2H_5OH, as shown in Fig. 6c, went through a maximum at 250 °C for all the nanoparticles. The response of bare-SnO_2 to C_2H_5OH was higher than that of Al-SnO_2 and Al_2O_3-SnO_2. The pore diameter of Al_2O_3-SnO_2 was larger than bare-SnO_2 (Fig. 3a), and the Al_2O_3-SnO_2 sensing layer was loosely packed. According to previous research, a porous sensing layer should give a higher sensor response to C_2H_5OH than densely packed sensing layer [5,32,33]. However, our sensor response to C_2H_5OH corresponded well with the oxygen adsorption amount. Zeng et al. suggested that C_2H_5OH rapidly reacts with adsorbed oxygen after adsorption and dissociation of the OH, as described in following equation [33]:

$$C_2H_5OH_{ads} + O^-_{ads} \rightarrow CH_3CHO + H_2O + e^- \quad (4)$$

According to the result shown in Fig. 5c, the SnO_2 surface has a high affinity to hydroxyls at 250 °C. Thus, the hydrophilic surface of SnO_2 is very effective for C_2H_5OH sensing because of a reaction (Equation 4) occurring at low operating temperatures. Additionally, the C_2H_5OH combustion reaction consumes the adsorbed oxygen by successive reactions, as described in previous reports using Pt/Rh/SnO_2 [7] and Sc/In_2O_3 [34]. Although they suggested various pathways for the combustion reaction, the clear root of the surface reaction on the bare-SnO_2 is still not clear. Nevertheless, such successive reactions enhance the sensor response to C_2H_5OH, and our SnO_2 sensors were more sensitive to C_2H_5OH than to H_2 and CO. Therefore, increasing the oxygen adsorption amount is important to enhance the sensor response by accelerating the combustion reaction. Additionally, the sensor response to C_2H_5OH is much higher than that of various SnO_2 based semiconductor gas sensors in the literature [4-6,32,33].

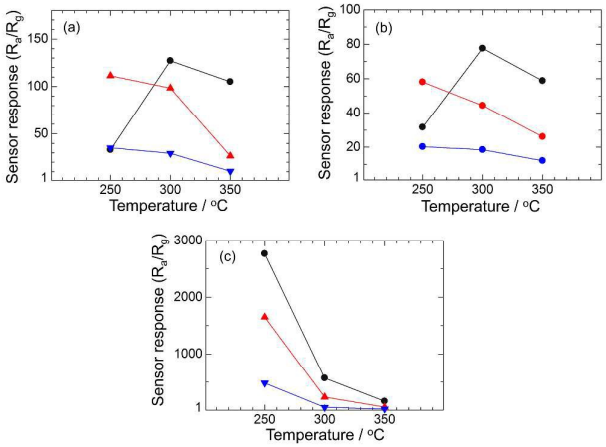

Fig. 6 The sensor response to (a) 200 ppm H_2, (b) 200 ppm CO, and (c) 100 ppm C_2H_5OH in dry atmosphere as a function of operating temperature using (●) bare-SnO_2 nanoparticles, (▲) Al-doped SnO_2 nanoparticles, and (▼) Al_2O_3-loaded SnO_2 nanoparticles.

Figure 7a–c shows the temperature dependence of the sensor response to H_2 and CO (200 ppm) and C_2H_5OH (100 ppm) in a humid atmosphere (45 % R.H. at 25 °C). The sensor responses deteriorated significantly compared with that in a dry atmosphere because of hydroxyl poisoning. The sensor responses to H_2 and CO increased with temperature in all the materials. Increasing the temperature leads to desorption of hydroxyls, resulting in an increase of adsorbed oxygen. Accordingly, the surface reaction rate increases with temperature. For C_2H_5OH, the response went through a maximum at 300 °C because C_2H_5OH is reactive at a lower temperature than H_2 and CO, similar to that observed in the dry atmosphere. This result indicates that the amount of residual adsorbed oxygen at 300 °C is more effective than that at 350 °C. Amazingly, bare-SnO_2 shows almost no sensitivity to the target gases at 250 and 300 °C because of its high affinity to hydroxyls. This lack of sensitivity indicates that almost no adsorbed oxygen exists on the particle surface. Most importantly, the sensor response using Al-SnO_2 and Al_2O_3-SnO_2 nanoparticles was higher than bare-SnO_2 nanoparticles for all of the target gases. Such a high sensor response implies a large amount of oxygen adsorption. Hence, these results indicate that Al and Al_2O_3 inhibit hydroxyl poisoning on the oxygen adsorption site. This phenomenon is well explained by the humidity-interference effect and the introduction of a hydroxyl absorber on the SnO_2 nanoparticles, as described earlier for NiO-doped SnO_2 [21]. Al and Al_2O_3 act as a water vapour absorber on the SnO_2 surface. Additionally, the sensor response to H_2 and CO in a humid atmosphere using Al-SnO_2 nanoparticles is comparable with that of Pd-loaded SnO_2 [20] and NiO-doped SnO_2 [21] gas sensors, respectively. For C_2H_5OH, the sensor response using Al-SnO_2 nanoparticles is higher than that of porous SnO_2 gas sensors [35,36], even though the humidity of these measurement is lower than our measurement. The sensor responses to C_2H_5OH using Al-SnO_2 nanoparticles were 2.7 times higher than that of Al_2O_3-SnO_2 nanoparticles at 300 °C, respectively. The crystallite size and specific surface area of Al_2O_3-SnO_2 were not suitable for obtaining a high sensor response. Additionally, we believe that Al in Al-SnO_2 is more highly dispersed in Al_2O_3 in Al_2O_3-SnO_2 because of the aggregation of Al_2O_3 (Fig. 4). Hence, highly dispersed Al

effectively absorbs hydroxyls and accelerates oxygen adsorption on the SnO_2 surface. Thus, the sensor response to combustible gases in a humid atmosphere was enhanced.

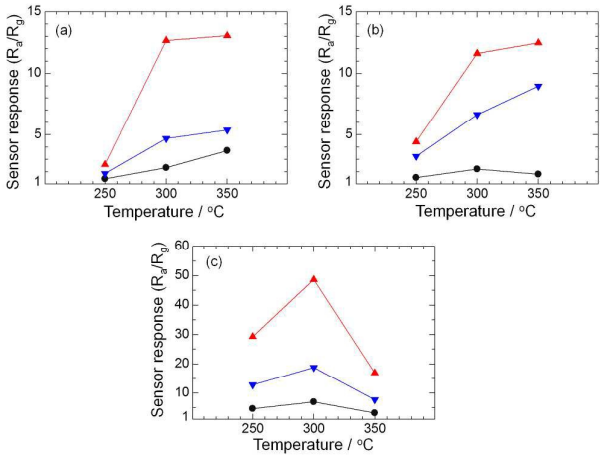

Fig. 7 The sensor response to (a) 200 ppm H_2, (b) 200 ppm CO, and (c) 100 ppm C_2H_5OH in humid atmosphere (45 % R.H. at 25 °C) as a function of operating temperature using (●) bare-SnO_2 nanoparticles, (▲) Al-doped SnO_2 nanoparticles, and (▼) Al_2O_3-loaded SnO_2 nanoparticles.

Figure 8 shows the sensor response to C_2H_5OH as a function of C_2H_5OH concentration at 300 °C in a humid atmosphere (45% R.H. at 25 °C) using bare-SnO_2, Al-SnO_2, and Al_2O_3-SnO_2 nanoparticles. The sensor responses were clearly proportional to the C_2H_5OH concentration. According to the extrapolation line, it can be expected that Al-SnO_2 nanoparticles detect less than one ppm C_2H_5OH in a humid atmosphere. We believe that optimizing the Al doping amount would give SnO_2-based materials a more sensitive surface in a humid atmosphere.

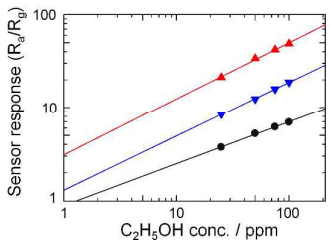

Fig. 8 The C_2H_5OH concentration dependence of the sensor response at 300 °C in humid atmosphere, using (●) bare-SnO_2 nanoparticles, (▲) Al-doped SnO_2 nanoparticles, and (▼) Al_2O_3-loaded SnO_2 nanoparticles.

Conclusions

We have successfully developed highly sensitive, surface-modified SnO_2 nanoparticles incorporating Al and Al_2O_3 that demonstrate resistance to humidity. Spherical bare-SnO_2, Al-SnO_2, and Al_2O_3-SnO_2 nanoparticles were prepared using conventional methods. XRD, TEM, surface analysis, and SEM suggest that the bare-SnO_2 nanoparticle and Al-SnO_2 nanoparticle are similar in size while the Al_2O_3-SnO_2 is larger. The amount of oxygen adsorbed by bare-SnO_2 was clearly greater than that adsorbed by Al-SnO_2 and Al_2O_3-SnO_2, as confirmed by O_2-TPD measurement. Bare-SnO_2 adsorbed more oxygen because it has a high affinity to oxygen ions. In addition, the dispersity of Al in Al-SnO_2 was higher than that of Al_2O_3 in Al_2O_3-SnO_2. The sensor responses to combustible gases using Al-SnO_2 and Al_2O_3-SnO_2 were lower than bare-SnO_2 in a dry atmosphere because incorporating Al reduces the combustion reaction rate with adsorbed oxygen. Conversely, in a humid atmosphere, the response to combustible gases using Al-SnO_2 was approximately five to ten times larger than bare-SnO_2. Al_2O_3-SnO_2 also showed a higher sensor response to combustible gases than bare-SnO_2. These results indicate that Al and Al_2O_3 inhibit hydroxyl poisoning of SnO_2 nanoparticles by working as hydroxyl absorbers and producing an oxygen adsorption site around them. The Al doping process dispersed Al in SnO_2 nanoparticles discretely, leading to an effective surface for combustion reactions in a humid atmosphere. Additionally, it was expected that Al-SnO_2 can detect C_2H_5OH at ppb levels in a humid atmosphere. Therefore, Al doping offers a better surface for combustible gas sensors in a humid atmosphere. These results suggest surface modification as a possible improvement for material design. We believe that further modification of Al-SnO_2, such as morphological regulation and catalytic addition, would create attractive materials for humidity-tolerant semiconductor gas sensors. Therefore, further development of these materials will enable development of the high performance gas sensors with resistance to poisoning gases and more compact gas sensors than are currently available.

Acknowledgment

This work was supported in part by the FIST Foundation for Interaction in Science & Technology, Japan.

Notes and references

1 T. Kida, S. Fujiyama, K. Suematsu, M. Yuasa, K. Shimaoe, Pore and Particle Size Control of Gas Sensing Films Using SnO_2 Nanoparticles Synthesized by Seed-Mediated Growth: Design of Highly Sensitive Gas Sensors. *J. Phys. Chem. C*, 2013, **117**, 17574-17582.
2 K. Suematsu, Y. Shin, Z. Hua, K. Yoshida, T. Kida, K. Shimanoe, Nanoparticle Cluster Gas Sensor: Controlled Clustering of SnO_2 Nanoparticles for Highly Sensitive Toluene Detection. *ACS Appl. Mater. Interfaces*, 2014, **6**, 5319-5326.
3 D. Flak, A. Braun, B.S. Mun, J.B. Park, M. Parlinska-Wojtan, T. Graule, M. Rekas, Spectroscopic Assessment of the Role of Hydrogen in Suface Defects, in the Electronik Structure and Transport Properties of TiO_2, ZnO and SnO_2 Nanoparticles. *Phys. Chem. Chem. Phys.*, 2013, **15**, 1417-1430.
4 A. Kar, A. Patra, Recent Development of Core-Shell SnO_2 Nanostructures and Their Potential Applications. *J. Mater. Chem. C*, 2014, **2**, 6707-6722.
5 Y. Liu, Y. Jiao, Z. Zhang, F. Qu, A. Umar, X. Wu, Hierarchical SnO_2 Nanostructures Made of Intermingled Ultrathin Nanosheets for Environmental Remediation, Smart

Gas Sensor, and Supercapacitor Applications. *ACS Appl. Mater. Interfaces*, 2014, **6**, 2174-2184.

6 V.V. Kovalenko, M.N. Rumyantseva, A.M. Gaskov, E.V. Makshina, V.V. Yushchenko, I.I. Ivanova, A. Ponzoni, G. Faglia, E. Comini, SnO_2/Fe_2O_3 Nanocomposites: Ethanol-Sensing Performance and Catalytic Activity for Oxidation of Ethanol. *Inorg. Mater.*, 2006, **42**, 1088-1093.

7 A. Kowal, M. Li, M. Shao, K. Sasaki, M.B. Vukmirovic, J. Zhang, N.S. Marinkovic, P. Liu, A.I. Frenkel, R.R. Adzic, Ternary Pt/Rh/ SnO_2 electrocatalysts for oxidizing ethanol to CO_2. *NAT. MATER.*, 2009, **8**, 325-330.

8 N. Kamiuchi, T. Mitsui, N. Yamaguchi, H. Muroyama, T. Matsui, R. Kikuchi, K. Eguchi, Activation of Pt/SnO_2 Catalyst for Catalytic Oxidation of Volatile Organic Compounds. *Catal. Today*, 2010, **157**, 415-419.

9 Y. Duan, J. Zheeng, N. Fu, Y. Fang, T. Liu, Q. Zhang, X. Zhou, Y. Lin, F. Pan, Enhancing the Performance of Dye-Sensitized Solar Cells: Doping SnO_2 Photoanodes with Al to Simultaneously Improve Conduction Band and Electron Lifetime. *J. Mater. Chem. A*, 2015, **3**, 3066-3073.

10 T. Jia, W. Wang, F. Long, Z. Fu, H. Wang, Q. Zhang, Synthesis, Characterization, and Photocatalytic Activity of Zn-Doped SnO_2 Hierarchical Architectures Assembled by Nanocones. *J. Phys. Chem. C*, 2009, **113**, 9071-9077.

11 X. Duo, D. Sabba, N. Mathews, L. Helena, Y.M. Lam, S. Mhaisalkar, Hydrothermal Synthesis of High Electron Mobility Zn-doped SnO_2 Nanoflowers as Photoanode Material for Efficient Dye-Sensitized Solar Cells. *Chem. Mater.*, 2011, **23**, 3938-3945.

12 J. Zhu, Z. Lu, S.T. Aruna, D. Aurbach, A. Gedanken, Sonochemical Synthesis of SnO_2 Nanoparticles and Their Preliminary Study as Li Insertion Electrodes. *Chem. Mater.,* 2000, **12**, 2557-2566.

13 T. Kida, T. Kuroiwa, M. Yuasa, K. Shimanoe, N. Yamazoe, Study on the Response and Recovery Properties of Semiconductor Gas Sensors Using a High-Speed Gas-Switching System. *Sens. Actuator B*, 2008, **134**, 928-933.

14 K. Suematsu, Y. Shin, N. Ma, T. Oyama, M. Sasaki, M. Yuasa, T. Kida, K. Shimanoe, Pulse-Driven micro Gas Sensor Fitted with Clustered Pd/SnO_2 Nanoparticles. *Anal. Chem.*, 2015, DOI: 10.1021/acs.analchem.5b01767.

15 R. Triantafyllopoulou, C. Tsamis, Detection of CO and NO Using Low Power Metal Oxide Sensors. *phys. Stat. sol.*, 2008, **205**, 2643-2646.

16 D. Koziej, N. Barsan, U. Weimar, J. Szuber, K. Shimanoe, N. Yamazoe, Water-Oxygen Interplay on Tin Dioxide Surface: Inplication on Gas Sensing. *Chem. Phys. Lett.*, 2005, **410**, 321-323.

17 N. Yamazoe, J. Fuchigami, M. Kishikawa, T. Seiyama, Interaction of Tin Oxide Surface with O_2, H_2O and H_2. *Surf. Sci.*, 1979, **86**, 335-344.

18 R.G. Pavelko, H. Daly, C. Hardacre, A.A. Vasiliev, E. Llobet, Interaction of Water, Hydrogen and Their Mixtures with SnO_2 Based Materials: the Role of Surface Hydroxyl Groups in Detection Mecahnisms. *Phys. Chem. Chem. Phys.*, 2010, **12**, 2639-2647.

19 G. Korotchenkov, V. Brynzari, S. Dmitriev, Electrical Behavior of SnO_2 Thin Films in Humid Atmosphere., *Sens. Actuator B*, 1997, **54**, 197-201.

20 N. Ma, K. Suematsu, M. Yuasa, T. Kida, K. Shimanoe, Effect of Water Vapor on Pd-Loaded SnO_2 Nanoparticles Gas Sensor. *ACS Appl. Mater. Interfaces*, 2015, **7**, 5863-5869.

21 H.-R. Kim, A. Haensch, I.-D. Kim, N. Barsan, U. Weimar, J.-H. Lee, The Role of NiO Doping in Reducing the Impact of Humidity on the Performance of SnO_2-Based Gas Sensors: Synthesis Strategies, and Phenomenological and Spectroscopic Studies. *Adv. Funct. Mater.*, 2011, **21**, 456-4463.

22 K.-I. Choi, H.-J. Kim, Y.-C. Lang, J.-H. Lee, Ultraselective and ultrasensitive detection of H_2S in highly humid atmosphere using CuO-loaded SnO_2 hollow spheres for real-time diagnosis of halitosis. *Sens. Actuator B*, 2014, **194**, 371-376.

23 J.B. Peri, A Model for the Surface of γ-Alumina. *J. Phys. Chem.*, 1965, **69**, 220-230.

24 J. Szanyi, J.H. Kwak, R.J. Chimentao, C.H.F. Peden, Effect of H_2O on the Adsorption of NO_2 on γ-Al_2O_3: an in Situ FTIR/MS Study. *J. Phys. Chem.*, 2007, **111**, 2661-2669.

25 T. Shirai, J.W. Li, K. Matsumaru, C. Ishizaki, K. Ishizaki, Surface Hydration States of Commercial High Purity α-Al_2O_3 Powders Evaluated by Temperature Programmed Desorption Mass Spectrometry and Diffuse Reflectance Infrared Fourier Transform Spectroscopy. *Sci. Technol. Adv. Mater.*, 2005, **6**, 123-128.

26 K. Suematsu, M. Yuasa, T. Kida, N. Yamazoe, K. Shimanoe, Effects of Crystallite Size and Donor Density on the Sensor Response of SnO_2 Nano-Particles in the State of Volume Depletion. *J. Electrochem. Soc.*, 2012, **159**, J136-J141.

27 S.J. Huang, A.B. Walters, M.A. Vannice, TPD, TPR and DRIFT Studies of Adsorption and reduction of NO on La_2O_3 dispersed on Al_2O_3. *Appl. Catal. B,* 2000, **26**, 101-118.

28 E.S. Putna, J.M. Vohs, R.J. Gorte, Evidence for Weakly Bound Oxygen on Ceria Films. *J. Phys. Chem.*, 1996, **100**, 17862-17865.

29 S. Singkammo, A. Wisitsoraat, C. Sriprachuabwong, A. Tuantranont, S. Phanichphant, C. Liewhiran, Electrolytically Exfoliated Graphene-Loaded Flame-Made Ni-Doped SnO_2 Composite Film for Acetone Sensing. *ACS Appl. Mater. Interfaces*, 2015, **7**, 3077-3092.

30 N. Yamazoe, K. Shimanoe, Role of Shape and Size of Component Crystals in Semiconductor Gas Sensors II. Response to NO_2 and H_2. *J. Electrochem. Soc.*, 2008, **155**, J93-J98.

31 G. Sakai, N. Matsunaga, K. Shimanoe, N. Yamazoe, Theory of Gas-Diffusion Controlled Sensitivity for Thin Film Semiconductor Gas Sensor. *Sens Actuator B*, 2001, **80**, 125-131.

32 J. Xu, Y.S. Li, H.T. Huang, Y.G. Zhu, Z.R. Wang, Z. Xie, X. Wang, D. Chen, G. Shen, Synthesis, Characterizations and Improved Gas-Sensing Performance of SnO_2 Nanospike Arrays. *J. Mater. Chem.*, 2011, **21**, 19086-19092.

33 W. Zeng, T. Li, T. Li, J. Hao, Y. Li, Template-Free Synthesis of Highly Ethanol-Response Hollow SnO_2 Spheres Using Hydrothermal Process. *J. Mater. Sci.: Mater. Electron*, 2015, **26**, 1192-1197.

34 M. Iwamoto, M. Tanaka, S. Hirakawa, S. Mizuno, M. Kurosawa, Pulse and IR Study on the Reaction Pathways for the Conversion of Ethanol to Propene over Scandium-Loaded Indium Oxide Catalysts. *ACS Catal.*, 2014, **4**, 3463-3469.

35 J. Zhang, J. Guo, H. Xu, B. Gao, Reactive-Template Fabrication of Porous SnO_2 Nanotubes and Their Remarkable Gas-Sensing Performance. *ACS Appl. Mater. Interfaces*, 2013, **5**, 7893-7898.

36 H. Zhang, W. Zeng, Y. Zhang, Y. Li, B. Miao, W. Chen, X. Peng, Synthesis and Gas Sensing Properties of Novel SnO_2 Nanorods. *J. Mater. Sci.: Mater. Electron*, 2014, **25**, 5006-5012.